Solvent-Induced Crystallization of Syndiotactic Polystyrene: Thermodynamics and Morphology

Biswajit Ray,[†] Said Elhasri,[‡] Annette Thierry, Pascal Marie, and Jean-Michel Guenet*

Institut Charles Sadron, CNRS UPR 22, 6, rue Boussingault, F-67083 Strasbourg Cedex, France

Received July 8, 2002; Revised Manuscript Received October 9, 2002

ABSTRACT: The thermodynamic properties and the morphology of syndiotactic polystyrene solid samples exposed to solvents (benzene and toluene) are investigated. It is shown that, as far as the melting properties are concerned, there is no significant difference between these samples and solution-cast samples. This suggests that compound formation is a near-equilibrium process in these systems. Conversely, the morphology depends on the sample thickness. Fibrillar networks are obtained with thin films as opposed to the various morphologies observed for bulk samples.

Introduction

Syndiotactic polystyrene (sPS), whose synthesis has been successfully carried out relatively recently,[1,2] possesses the propensity of forming polymer−solvent compounds (also designated as intercalates or crystallosolvates) in a large variety of solvents.[3−8] In this case the 2_1 helical structure is observed instead of the stabler planar zigzag.[3−5] In many cases these compounds are prepared by exposing a solid polymer sample to solvent liquid or solvent vapors which results in producing solid samples.[3,4] In other cases, compounds are prepared from homogeneous solutions obtained at high temperatures and cooled to lower temperatures[7,8] (solution-cast samples). In most cases this way of preparation leads to the formation of thermoreversible gels when fibrillar structures are formed or to pastelike systems when the growth of spherulites occurs.[5,6] For organized polymer−solvent systems prepared from homogeneous solutions, many thermodynamic studies dealing with the determination of the temperature−concentration phase diagram are available.[9−12] Conversely, in the case of solvent-exposed samples studies have been mainly focused on the short-range structure (the crystalline lattice) or on morphological aspects.[3−5] Also, to the best of our knowledge, a systematic study involving the exposure temperature and/or the thickness of the exposed solid polymer sample is still missing. This is the aim of this paper to report on such an investigation. In particular, we shall compare the melting behavior of solvent-exposed samples to that of samples prepared from homogeneous solutions. The morphology of samples obtained from bulk polymer and from polymer films will be compared.

Experimental Section

Materials. The syndiotactic polystyrene sample was synthesized following the method devised by Zambelli and coworkers.[2] ^{1}H NMR characterization showed that the content of syndiotactic triads was over 99%. The different moments of the molecular weight distribution were determined by GPC in dichlorobenzene at 140 °C. The following values were obtained: $M_w = 1.0 \times 10^5$ with $M_w/M_n = 4.4$.

Benzene and toluene were purchased from Aldrich and used without further purification.

Sample Preparation. The solvent-induced bulk samples were obtained in three steps: (i) molding of bubble-free disk-shaped pieces of semicrystalline syndiotactic polystyrene (20 mm diameter, 0.1 mm thickness) by heating at 270 °C under vacuum and cooling to room temperature; (ii) preparing amorphous samples by placing these samples between thin glass slides (in order to access rapid cooling rates when quenching), melting at 270 °C, and quenching into liquid nitrogen; (iii) exposure to liquid solvents at different temperatures. Under these conditions, disk-shaped samples with flat surfaces are obtained, which is a prerequisite for getting DSC thermogrammes of the highest possible quality.

Exposure times were approximately 1 month while keeping the samples in thermally regulated cells (±1 °C). A few samples were investigated after 6 months and 1 year exposure to liquid solvent but displayed no detectable differences with those exposed for 1 month.

The thin-layer samples were prepared in two steps: (i) Films of various thicknesses in the range from 70 to 250 nm were spin-coated onto methanol-washed glass slides at 500−4000 rpm from chloroform solutions of different concentrations. These films were melted again at 270 °C for 10 min and quenched at 0 °C within iced water. Under these conditions, sPS films were in the amorphous state. (ii) After removing water under vacuum, these films were exposed to toluene or benzene vapors at different temperatures for different times. Some samples were also prepared by dipping the films within the solvent. After appropriate exposure time, the excess solvent was soaked out with lint-free tissue, and the films were dried in air at room temperature. Films were also spin-coated on silicon wafers under the same conditions, and the single wavelength ellipsometry technique was used to determine their thickness.

Differential Scanning Calorimetry. DSC thermograms of the solvent-induced bulk samples were recorded by means of a Perkin-Elmer DSC 7. The samples were introduced into stainless steel sample pans that were hermetically sealed from the atmosphere. Loss of weight was checked after each experiment. Heating rates ranging from 5 to 20 °C were used. It is worth emphasizing that for each run a new sample was used on account of the irreversibility of the solvent-induced crystallization process. Irreversibility is taken here in the sense that after melting and cooling the second heating run

[†] Present address: Department of Applied Chemistry, Graduate School of Engineering, Nagoya University, Furo-cho, Chikusa-ku, Nagoya 464-8603, Japan.

[‡] Permanent address: Département de Physique, Faculté des Sciences et Techniques du Guéliz, Université Cadi-Ayyad, B.P 618, Marrakech, Morocco.

10.1021/ma0210731 CCC: $22.00
Published on Web 11/14/2002

does no longer correspond to a solvent-induced crystallization but to a crystallization from a highly concentrated solution instead.

Scanning Electron Microscopy. SEM experiments were performed on films dried at room temperature left on their glass or silicon supports. A conducting 80 nm thick coating gold layer was deposited by sputtering in an argon atmosphere. The observation of the surface topography was performed with a Hitachi S-2300 microscope operating at voltages ranging from 15 to 25 kV.

Atomic Force Microscopy. AFM experiments were carried out on the dried films at room temperature in air using a Nanoscope III instrument (Digital Instruments, Santa Barbara, CA). Most of the images reported in this work were obtained by means of the tapping mode (height and phase) with a silicon nitride cantilever (Olympus Optical Co. Ltd., Tokyo, Japan) having a spring constant of 42 N/m and a resonating frequency of 300 kHz. The scanning rates were varied from 1 to 2 Hz. All images presented in this work were obtained reproducibly over at least three spots on the sample surfaces.

Image Processing. From the original and global AFM image (1024 × 768 pixels size), the useful image (512 × 512 pixels size) of the structure is extracted and converted into black and white image. The digitized image was analyzed with Visilog Image Analysis Software (Noesis, France) using filtering techniques (smoothing for removing noise and sharpening for enhancing low contrasted images), mathematical morphology functions (merge_minima* and thinning, edge detection method), and adaptative thresholding to isolate the *black* domains corresponding to the mesh of the network and to locate the boundary (or edge) and interface contour of each domain considered as "particles" or "cells".[13−15] The cells at the edges of the binary image are removed, and the cells with hole(s) are filled for the determination of the area of cell. These particles can be analyzed so as to extract their dimensions (area, perimeter, diametrical variations and shape factor) and to determine their positions within the image (X and Y coordinates of the center of mass). A diameter is calculated from the corresponding area values A through $D = (4A/\pi)^{1/2}$.

Results and Discussion

Solvent-Induced Bulk Samples: Thermodynamics. The polymer fraction of the samples used for the DSC experiments, C_{pol}, has been determined by simply weighing the polymer left after drying by evaporation under vacuum at 50 °C. Infrared spectroscopy was used to ckeck the absence of any absorption bands related to the solvent. This procedure was achieved on all samples and showed a reproducibility of about ±5%. As will be discovered below, the polymer fraction decreases as the preparation temperature increases.

Typical DSC thermograms are given in Figure 1. As can be seen, three to four thermal events are easily identified: glass transition (T_g), compound melting transformation (C_m), recrystallization (R_c), and final melting (T_m). Before discussing further, it is worth stressing that polymer−solvent compounds are formed in both systems. This will become straightforward in what follows.

The occurrence of a glass transition reveals the presence of amorphous material. Values of T_g are significantly lower than those for pure polymer ($T_g^0 = 100 \pm 5$ °C), which points toward the presence of solvent in the amorphous domains, as is expected. Yet, in view of the values of T_g, the solvent fraction in these domains is most probably significantly lower than the global solvent fraction ($C_s = 1 - C_{pol}$). For instance, for a toluene-induced sample of global solvent fraction $C_s = 0.28$ ($C_{pol} = 0.72$), one observes $T_g = 60$ °C (see Figure 1). If one assumes that the variation of T_g of sPS as a function of the solvent fraction is likely to be closely identical to that of atactic polystyrene, for which experimental data are available,[16] then the solvent fraction in the amorphous domains is about 0.09. As the polymer concentration is always lower than $C_{pol} = 0.84$, this ultimately entails that the solvent fraction in the crystalline domains is higher, which is consistent with the occurrence of polymer−solvent compounds.

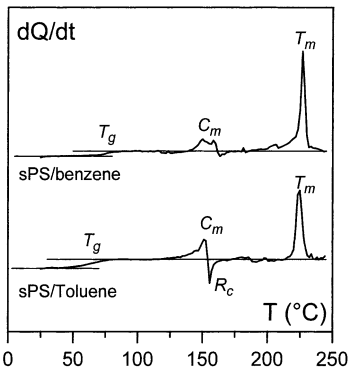

Figure 1. DSC thermograms for solid sPS samples (0.1 mm thick) exposed to liquid benzene (upper) and liquid toluene (lower). The various events are indicated (see text). In toluene exposure temperature $T_{expo} = 60$ °C, giving $C_{pol} = 0.71$ (w/w); in benzene exposure temperature $T_{expo} = 40$ °C, giving $C_{pol} = 0.82$ (w/w).

In principle, at C_m the compound ought to melt in an incongruent fashion (incongruently melting compound), which merely means that in the present cases the following transformation occurs:

$$\text{compound 1} + \text{compound 2} \Rightarrow \text{compound 2} + \text{liquid}$$

where compound 2 is less solvated than compound 1. Note that a limiting situation takes place when compound 2 is devoid of solvent molecules in which case this phase has to be designated as solid following the usual terminology. We shall find out in what follows that for sPS/toluene systems two compounds are involved.

At C_m transformation (1) therefore takes place, which results in solvent expulsion from compound 1. This should only produce an endothermic event. At the moment we can think of one possible reason for the occurrence of a recrystallization phenomenon (exotherm) just after the transformation endotherm: the difference of concentration between the crystalline phases and the amorphous domains. Availability of those solvent molecules expelled from compound 1 to the amorphous domains may promote the formation of an additional amount of compound 2 just after transformation (1), which would then produce an exothermic event. Recrystallization is less salient for benzene-induced compounds than for those induced from toluene. Recrystallization was not observed to this extent in the case of solution-cast samples from these two solvents, although it was reported to occur for sPS/chloroform systems.[8]

The data points for temperatures corresponding to the endothermic DSC events have been transferred onto the temperature−concentration phase diagrams previously established by Daniel et al. for solution-cast samples of these systems[7,8] (Figures 2 and 3). In the case of toluene

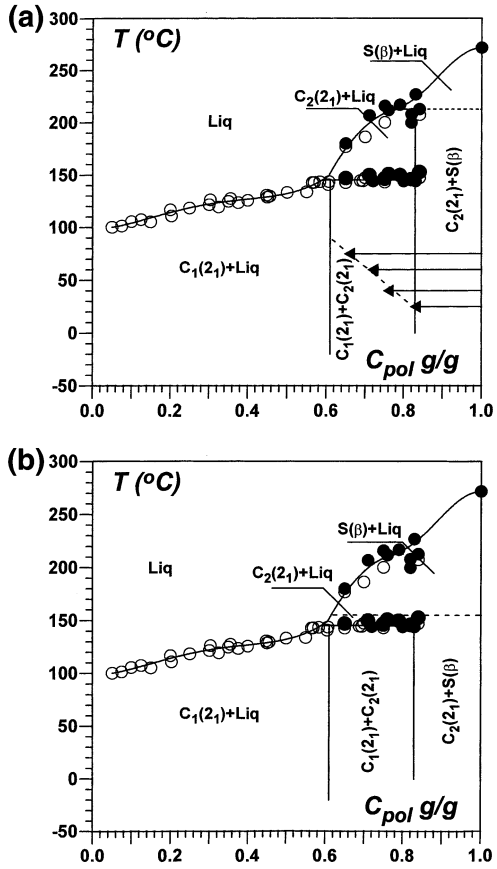

Figure 2. Temperature−concentration phase diagram for sPS/toluene systems. The open circles stand for solution-cast samples as determined by Daniel et al.;[8] the black circles represent data points obtained for solvent-exposed samples. The arrows indicate the overall concentration reached by the samples for different exposure temperatures (from bottom to top: 25, 40, 60, 75 °C). As usual, the hypothetical transformations are indicated by dotted lines. Indications in brackets 2_1 and β stand for the solvated 2-fold helical structure and the nonsolvated planar zigzag form, respectively. Note that two diagrams are plausible with the available data (a and b). The main difference deals with the extension of the S(β) + Liq domain. In diagram b the transformation from C_1 into C_2 is immediately followed by a total desolvation process, thus producing $S(\beta)$.

all the data points gathered for solvent-induced samples are, within experimental uncertainties, virtually the same as those obtained from solution-cast samples. Clearly, the melting behavior and correspondingly the nature of the phases do not depend significantly upon the path followed to reach a given C_{pol}, T coordinate: starting from concentration C and cooling to temperature T is equivalent as starting from temperature T and reaching concentration C through solvent diffusion. It is also worth mentioning that this statement also applies to the latent heats ΔH associated with thermal events C_m and T_m: whenever a good baseline in DSC traces permits determination with sufficient accuracy of these quantities, they correspond within experimental uncertainties to those measured from solution-cast samples. The systems therefore behave as if they were at equilibrium, an outcome that was certainly not obvious. This emphasizes again that rules deduced from equilibrium thermodynamics, especially Gibbs phase rules for establishing phase diagrams, can be used to describe systems that are not strictly speaking at equilibrium.[17]

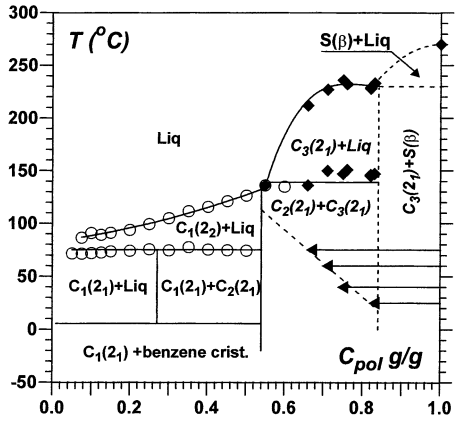

Figure 3. Temperature−concentration phase diagram for sPS/benzene systems. The open circles stand for solution-cast samples as determined by Daniel et al.;[7] the black circles represent data points obtained for solvent-exposed samples. The arrows indicate the overall concentration reached by the samples for different exposure temperatures (from bottom to top: 25, 40, 60, 75 °C). As usual, the hypothetical transformations are indicated by dotted lines. Indications in brackets 2_1 and β stand for the solvated 2-fold helical structure and the nonsolvated planar zigzag form, respectively.

Note that the domain where $S(\beta)$ and the liquid coexist can be different whether the transformation C_2 into $S(\beta)$ takes place just after the melting of compound C_1 or at much higher temperature. This would imply that at 150 °C only the $S(\beta)$ crystalline phase would exist as was for instance observed for sPS/*o*-xylene systems.[18] There is a lack of unambiguous data for settling definitely this point so that the two possibilities are given in Figure 2.

As expected, the final concentration reached by the system depends on the temperature at which the solid polymer has been exposed to the solvent: the higher the exposure temperature T_{expo}, the lower the polymer fraction. This is highlighted in the phase diagram by means of arrows (Figure 2). The evolution of C_{pol} vs T_{expo} appears to be linear (dotted line joining arrows). This also implies that polymer concentrations lower than $C_{pol} \approx 0.48$ cannot be reached by solvent exposure without melting and dispersing into the solvent the initially solid polymer sample. Indeed, at a temperature $T_{expo} \approx 130$ °C, the liquid phase is obtained in a sealed vessel (total dissolution of the polymer).

In the case of benzene, polymer concentrations higher than those achieved by Daniel et al. from solution-cast systems have been obtained.[7] It, however, seems that the data points obtained from the solvent-induced systems in the range of high polymer concentrations complete the phase diagram established for solution-cast samples. If so, the melting events and the corresponding phases are, like with toluene, independent of the processing path.

As with toluene, the polymer concentration varies linearly with the exposure temperature (as shown by arrows in Figure 3). Joining the arrows with a straight line suggests that compound C_1, the compound of highest degree of solvation, cannot be prepared by solvent exposure of a solid piece of polymer as one would one end up with $T_{expo} \approx 190$ °C, a temperature at which a homogeneous solution would be formed before any compound formation could take place.

We note that the highest concentration achieved for sPS/benzene systems ($C_{pol} = 0.82$) would correspond to

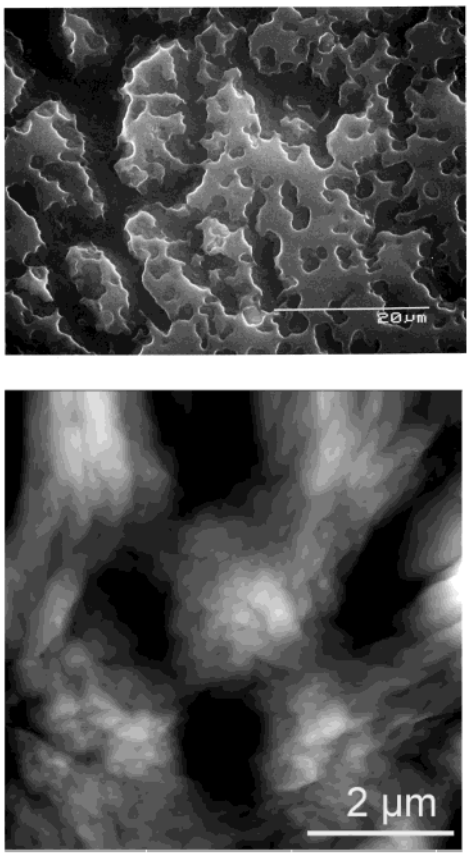

Figure 4. Scanning electron micrograph (top) and AFM image (bottom) of the surface of a thick sPS solid sample exposed to benzene at 40 °C.

a compound of stoichiometry 4/1 (4 monomers for 1 solvent molecules). In the case of toluene the highest polymer concentration that has been reached corresponds to the stoichiometric composition of the 4/1 compound identified by Chatani and co-workers.[5] It is quite likely that benzene forms the same type of compound. That the melting temperatures tend to level off in this composition range is consistent with the occurrence of a third compound, although the existence of compound C_3 remains hypothetical with the data at hand. Note that as with toluene the extension of the domain S(β) + liquid can be much larger if the transformation C_3 into S(β) occurs near 150 °C.

Apparently, the absorption of solvent in both systems is restricted to polymer concentrations corresponding to the compound of stoichiometric concentration 1 solvent molecule/monomer. Possibly, an increase of pressure could modify this limit. This remains to be tested.

Solvent-Induced Bulk Samples: Morphology. The surface morphology of the solvent-induced samples has been studied by SEM and AFM microscopy. Typical pictures are given for sPS/benzene systems for two temperatures in Figures 4 and 5. For samples exposed at T_{expo} = 25 °C (Figure 4a) and T_{expo} = 40 °C (not shown), the surface looks highly corroded as would happen under the effect of chemicals. As no chemical modification takes place, this effect can be better described as a "physical corrosion". AFM allows higher resolution to be achieved, yet a "fluffy" aspect still shows up (Figure 4b). It is not clear whether spherulites are formed. At higher temperature (T_{expo} = 75 °C, Figure 5a), a moonlike aspect is observed by SEM. The formation of craters may stem from the fact that this temperature is close to benzene's boiling point. A closer look through AFM reveals lamellar morphology in some parts of the sample (Figure 5b).

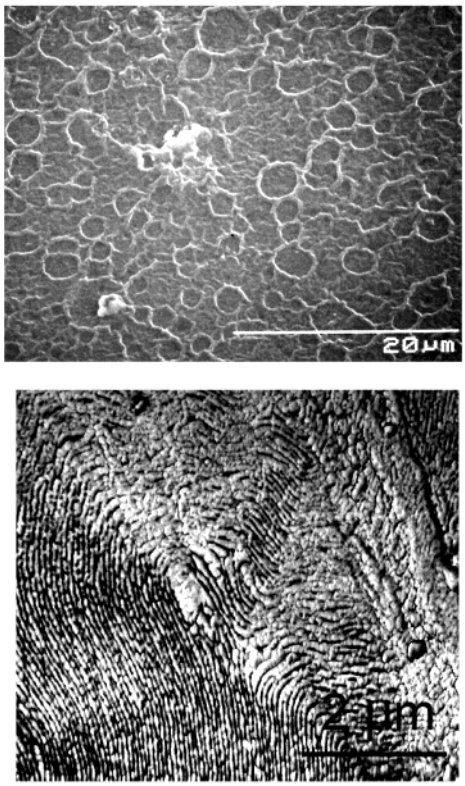

Figure 5. Scanning electron micrograph (top) and AFM image (bottom) of the surface of a thick sPS solid sample exposed to benzene at 75 °C.

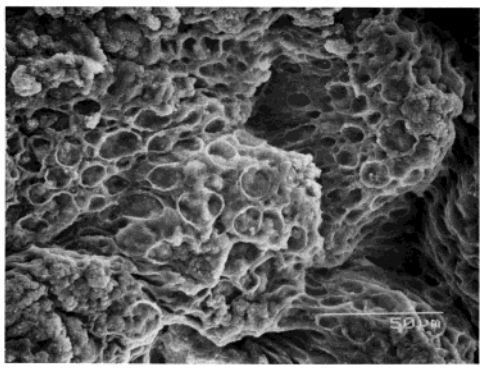

Figure 6. Scanning electron micrograph of the surface of a thick sPS solid sample exposed to benzene at 90 °C.

At T = 90 °C, which is some 15 °C above the benzene boiling point, the crater morphology is still more pronounced (Figure 6).

Conversely, for toluene-exposed samples a coarse grain structure, already reported by Vittoria et al.,[4] is always seen in the range 25−90 °C (see Figure 7).

Thin-Layer Samples: Morphology. The morphology of thin-layer samples differs considerably from that of the bulk samples. As can be seen in Figure 8, a fibrillar network morphology is obtained in both solvents independent of the exposure temperature and of the use of solvent vapor or solvent liquid. The typical mesh size of these fibrillar networks lies somewhere between 0.1 and 1 μm. These figures are quite reminiscent of those reported for gels prepared from solution-cast samples.[7,8] As shown in Figure 9, although the

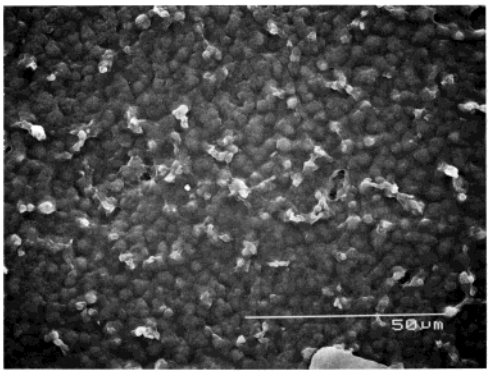

Figure 7. Scanning electron micrograph of the surface of a thick sPS solid sample exposed to toluene at 75 °C.

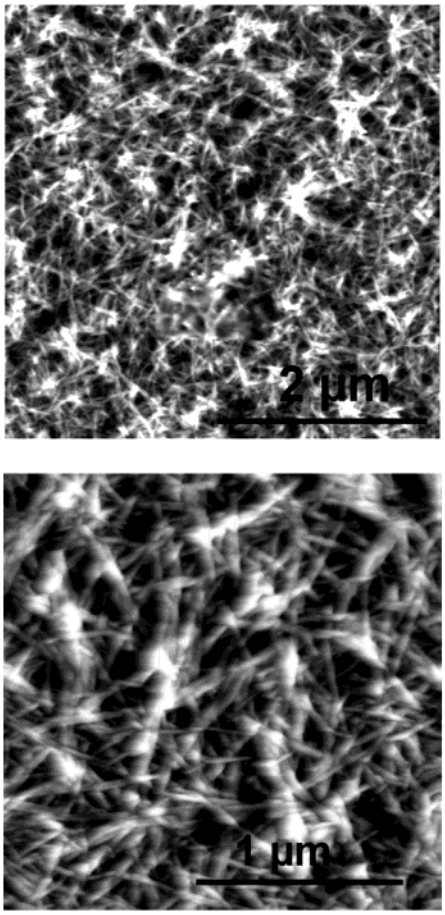

Figure 8. AFM images of thin sPS films (in both cases initial thickness = 0.2 μm) exposed to benzene at 75 °C (top) and to toluene at 90 °C (bottom).

starting layer presents some roughness, the resulting fibrillar structures do not arise from any underlying "order" generated during the thin-layer preparation. Also, it can be observed that the final structure is reached after a relatively short exposure time.

Admittedly, the way the samples are prepared has a dramatic effect on the resulting structures. It is worth mentioning that some properties, such as the glass transition temperature, are known to be dependent upon the layer thickness.[19] The difference between bulk samples and thin layer samples may therefore arise from a sample size effect.

That fibrillar networks are formed, in other words highly porous structures, suggests that the concentration reached after solvent-exposure is significantly lower than those achieved with bulk samples. Indeed, if polymer concentrations have values above the stoichiometric concentration of any compound, then no porosity should be observed. This is so because one is then dealing with two solid crystalline phases while the occurrence of porosity requires the existence of a polymer-poor liquid phase. Clearly, concentrations substantially smaller than $C_{pol} = 0.6$ for sPS/toluene mixtures and $C_{pol} = 0.27$ for sPS/benzene systems must be reached in order to create the required liquid phase. One possible mechanism consists of postulating that the system goes through a "homogeneous solution" state before compound formation sets in. This highly solvated state may be accessed on account of the thinness of the sample which makes it easier for the solvent to diffuse and dissolve the polymer.

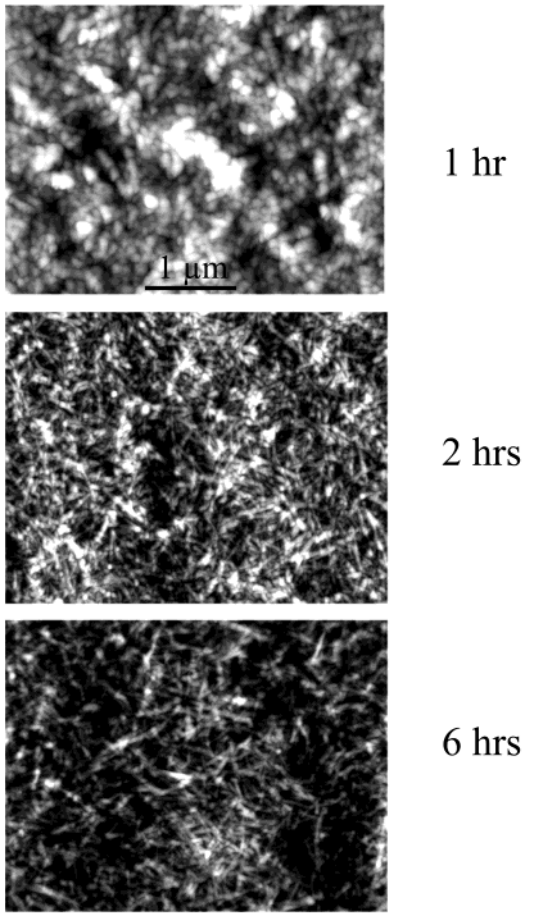

Figure 9. AFM images of a thin sPS films (initial thickness = 0.15 μm) exposed to toluene at 75 °C for different times (as indicated). Each image corresponds to a different sample.

Thin-Layer Samples: Porosity. From the AFM picture a deeper analysis of the mesh size of the fibrillar network has been carried out. It has been assumed that the size of the holes (darkest parts of the image) is related to the mesh size of the fibrillar networks. Under these conditions some comparison can be made between different samples although the actual mesh size is not directly accessible from these experiments. The way the binary digitization of the image has been performed,[13−15] namely transforming the initial gray level image into black spots (the holes) and white continuum (the continuous phase), is shown in Figure 10. Typical histograms of the frequency of the different diameters are given in Figure 11. These histograms have been

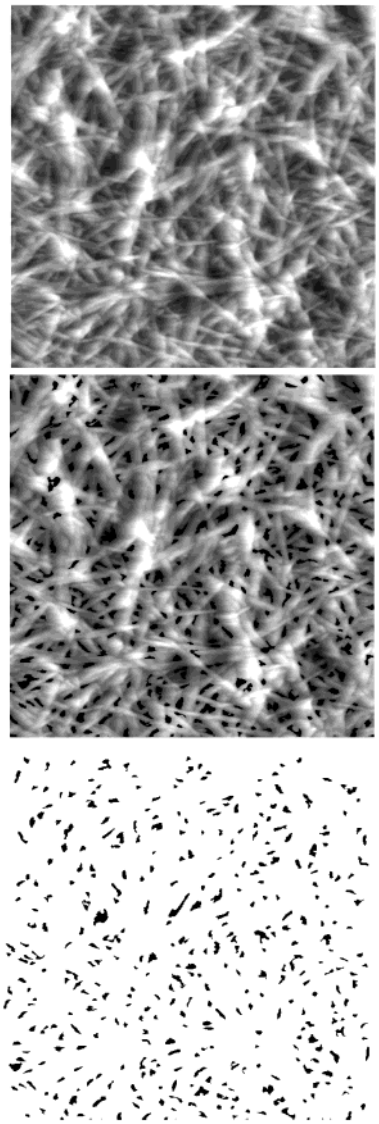

Figure 10. The three-step image processing for determining the size and distribution of the darkest spots that are supposed to be related to the mesh size of the network.

fitted with the following log-normal distribution:

$$X(D) = \frac{A}{\sigma_g D \sqrt{2\pi}} \exp\left[-\frac{(\ln(D/D_m)^2}{2\sigma_g{}^2}\right] \quad (1)$$

in which

$$\sigma_g{}^2 = \int (\log D - \log D_m)^2 X(D)\, dD \quad (2)$$

and

$$\log D_m = \int \log D X(D)\, dD \quad (3)$$

where A is the amplitude and $X(D)$ is the probability density function (frequency function) of the diameters D. D_m is a mean diameter defined through

$$\int_0^{D_m} X(D)\, dD = 1/2 \quad (4)$$

The fits are given for two exposure temperatures in toluene, namely 25 and 75 °C. Clearly the mesh size at 25 °C appears to be smaller by a factor of about 2 with

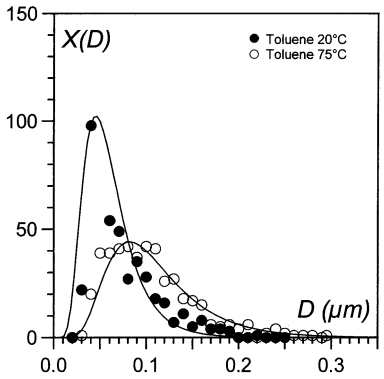

Figure 11. Frequency function $X(D)$ vs D of the diameters of the darkest spots in processed images of the type shown in Figure 10. In both cases thin sPS films (initial thickness = 0.2 μm) exposed to toluene at two different temperatures (○ for T_{expo} = 75 °C; ● for T_{expo} = 25 °C).

regards to samples prepared at 75 °C. The present analysis highlights the role of the exposure temperature for monitoring the porosity of the samples. That the porosity is larger for T_{expo} = 75 °C than for T_{expo} = 25 °C is not surprising as the overall polymer concentration is supposed to decrease with increasing the exposure temperature, thus augmenting the poor-polymer phase (the liquid phase) proportion.

Concluding Remarks

The present investigation has highlighted two major points. The first deals with the thermodynamics of the formation of the compounds through solvent exposure. We have observed that the melting behavior is not significantly influenced by the path used for preparing the compounds: cooling to low temperature hot homogeneous solutions or allowing the solvent to diffuse at constant temperature in a solid polymer matrix give nearly identical results. This was not at all obvious and shows that Gibbs phase rules for establishing phase diagrams that were originally established for systems at equilibrium can still be applied to systems that are not strictly speaking at equilibrium. The second point deals with the thickness of the solid polymer sample exposed to solvent. The morphology depends strongly on this parameter. In all cases a fibrillar morphology is produced when thin films are used. The porosity of the networks appears to be determined by the temperature at which the samples are exposed. Conversely, the morphology for bulk samples is not so clearly defined and depends on the solvent. This may be so because polymer concentrations reached for bulk polymer samples may be much higher than those achieved for thin films. In the latter case the occurrence of a liquid phase (polymer-poor phase) is likely to be promoted, which in turn will permit the formation of a fibrillar network close to the morphology observed for similar systems in the case of low polymer concentrations.

Acknowledgment. Dr. Biswajit Ray is greatly indebted to the French Government (Ministère de la Recherche) for a postdoctoral grant in aid.

References and Notes

(1) Ishihara, N.; Seimiya, T.; Kuramoto, M.; Uoi, M. *Macromolecules* **1986**, *19*, 2465.
(2) Grassi, A.; Pellechia, P.; Longo, P.; Zambelli, A. *Gazz. Chim. Ital.* **1987**, *117*, 249.

(3) Immirzi, A.; de Candia, F.; Ianelli, P.; Zambelli, A.; Vittoria, V. *Makromol. Chem. Rapid Commun.* **1988**, *9*, 761.
(4) Vittoria, V.; de Candia, F.; Ianelli, P.; Immirzi, A. *Makromol. Chem. Rapid Commun.* **1988**, *9*, 765.
(5) Chatani, Y.; Shimane, Y.; Inagaki, T.; Ijitsu, T.; Yukinari, T.; Shikuma, H. *Polymer* **1993**, *34*, 1620.
(6) Guerra, G.; Vitagliano, V. M.; De Rosa, C.; Petraccone, V.; Corradini, P. *Macromolecules* **1990**, *23*, 1539.
(7) Daniel, C.; De Luca, M. D.; Brûlet, A.; Menelle, A.; Guenet, J. M. *Polymer* **1996**, *37*, 1273.
(8) Daniel, C.; Brûlet, A.; Menelle, A.; Guenet, J. M. *Polymer* **1997**, *38*, 4193.
(9) Smith, P.; Pennings, A. J. *Polymer* **1974**, *15*, 413.
(10) Wittmann, J. C.; St John Manley, R. *J. Polym. Sci., Polym. Phys. Ed.* **1977**, *15*, 1089.
(11) Point, J. J.; Coutelier, C. *J. Polym. Sci., Polym. Phys. Ed.* **1984**, *22*, 231.
(12) Guenet, J. M.; McKenna, G. B. *Macromolecules* **1988**, *21*, 1752.
(13) Coster, M.; Chermant, J. L. *Précis d'Analyse d'Images*; Presses du CNRS: Paris, 1979.
(14) Serra, J. *Image Analysis and Mathematical Morphology*; Academic Press: New York, 1983.
(15) Soille, P. *Morphology Image Analysis;* Springer-Verlag: Berlin, 1999.
(16) Braun, G.; Kovacs, A. In *Physics of Non-crystalline Solids;* Proc. Int. Conf. Delft; North-Holland Publ. Co.; Amsterdam, 1964.
(17) Guenet, J. M. *Thermochim. Acta* **1996**, *284*, 67.
(18) Deberdt, F.; Berghmans, H. *Polymer* **1994**, *35*, 1694.
(19) See for instance: Van der Lee, A.; Hamon, L.; Holl, Y.; Grohens, Y. *Langmuir* **2001**, *17*, 7664.

MA0210731